International Journal of Tomography & Statistics,
Winter 2010, Vol. 13, No. W10; Int. J. Tomogr. Stat.,
ISSN 0972-9976 (Print); ISSN 0973-7294 (Online)

Automatic Cropping for LV Segmentation in Cardiac MRI

Isabela Silva[1]*, **Ana G. Almeida**[2] **and João Sanches**[1]

[1]Institute for Systems and Robotics
Instituto Superior Técnico
1049-001 Lisbon, Portugal

[2]Faculdade de Medicina da Universidade de Lisboa
1649-028 Lisbon, Portugal

ABSTRACT

Left ventricle (LV) contour extraction and tracking is important in diagnosis of cardiac pathologies. This procedure is difficult, is usually performed manually using software assistance, is time consuming and presents high intra/inter operator variability. Automatization of this process is of great importance to the clinical practice.

The most state of the art algorithms for LV segmentation, described in the literature, are semi-automatic allowing to reduce significantly the human intervention. A full automatic approach is still an open problem mainly because it is difficult to compute a good initial guess for the contour, close enough of the final solution. Additionally, since the total amount of available data is usually large, and the *region of interest* (ROI) containing the LV is smaller than the overall acquired volume, an automatic crop is needed to reduce the computational burden associated with the pre-processing and segmentation algorithms. The pre-processing performs compensation in one hand, for coil sensitivity that induces intensity fluctuations across the images and, in the other hand, for misalignments due small movements during the breath-hold acquisition protocol.

In this paper we propose an algorithm to automatically crop the acquired volume by defining an adaptive size ROI containing the LV. This cropping is based on the well known Hough transform for circles, in the prior knowledge about the location of the heart and also on the high signal variability over time due to muscle contraction at the LV borders.

Tests with real data have shown promising results.

Keywords: left ventricle, automatic crop, Hough transform.
2000 Mathematics Subject Classification: 68U10, 92C55.

1 Introduction

There are several non-invasive imaging techniques available to assess myocardial function, such as *echocardiography*, *single photon emission computed tomography* (SPECT), *positron emission tomography* (PET) and Magnetic Resonance Imaging (MRI).
MRI is one of the preferred diagnostic technique due to its high spatial resolution and soft-tissue contrast. Furthermore, despite the structural information, such as anatomy and tissue

*Corresponding author: Isabela Silva (isabela.silva@ist.utl.pt)

characterization, it provides the dynamic analysis such as perfusion, metabolism and function measurements in one single examination (Wu and Lima, 2003).

MRI is widely used to access cardiac *left ventricle* (LV) function and diagnose several heart pathologies. For instance, an important parameter used to evaluate LV function is the *ejection fraction* (EF) where the internal LV contour must be tracked during several cardiac cycles.

Usually, the physicians have to manually draw the LV contour from a stack of short-axis cine-MRI in systolic and diastolic time frames to compute the EF from these volumes. The volumes are usually composed by 10 up to 16 slices and 15 up to 30 images are acquired per cardiac cycle, corresponding to different phases of this cycle. Manually processing all this vast amount of data is time consuming and computer assistance is needed. Full automatic LV tracking and segmentation process is complex and still an open problem.

The acquired short-axis cine-MRI images present a series of obstacles that make this automatization a non-trivial problem: they are acquired over several breath-holds which can lead to the misalignment of the LV along the stack (Holland, Goldfarb and Edelman, 1998) and the signal intensity is not constant over the stack due to different sensitivity along the coil and over the slice due to cardiac flow dynamics (Pednekar, Muthupillai, Lenge, Kakadiaris and Flamm, 2006). These effects must be compensated by engaging in time consuming signal pre-processing. Therefore, a reduction of the original *field of view* (FOV) is needed to reduce the computational burden associated with the pre-processing, alignment and segmentation algorithms.

In this paper a full automatic 3D crop algorithm is proposed to select a sub-volume containing the LV in all images and in all temporal frames from the whole acquired data.

There are several semi-automatic LV segmentation algorithms described in the literature. In (Katouzian, Prakash and Konofagou, 2006) and in (Nascimento and Sanches, 2008; Nascimento and Marques, 2008) the operator must select a point in the image within the blood-pool of the LV.

Most of the proposed algorithms aiming at performing a fully automatic LV segmentation, usually follow two approaches to locate of the LV: i) they take into account the signal change over time due to muscle contraction (Cocosco, Netsch, Sénégas, Bystrov, Niessen and Viergever, 2004) or ii) they use the prior knowledge about the circular shape of the transversal cross sections of the LV (Müller, Neitmann, Merkle, Wohrle, Hombach and Kestler, 2005). Other approaches use multiple views to automatically identify the LV, such as the one proposed in (Pednekar et al., 2006).

In this work one important assumption is adopted and validated: although the heart orientation vary between exams, due to scanning protocols, the LV will never be found at the edges of the FOV and it is always close to the center of the image. The other assumptions adopted here, previously referred, are: the LV shape is circular and there is a high temporal variability of the image intensity in the myocardium boundaries. Under these assumptions, a fully automatic algorithm will be presented to calculate a ROI containing the LV.

Tests using real data have proven the robustness of the algorithm and its utility in the clinical practice.

This paper is organized as follows: Section 2 describes the image acquisition protocols and

the crop algorithm; Section 3 presents the results; Section 4 is used for discussion and main conclusions of this work.

2 Materials and method

2.1 MRI data

The presented algorithm was tested on 17 cardiac patients identified with letters from A to Q(five females and twelve males, mean age 48, ranging from 19 to 86) from *Sociedade Portuguesa de Ressonância Magnética* where the LV function was studied. The images were acquired on a 3T Philips scanner, using a Philips Sense cardiac six-channel coil. The cine-MRI study was gated to the ECG and acquired with steady state free precession image sequence. A series of 8 up to 14 short-axis slices encompassing all the LV length were acquired over 20 up to 30 time frames over the cardiac cycle. The slice thickness is of 7 mm with a 3 mm gap between them. The spacial resolution varies between 0.71 mm to 1.44 mm, normally with a value of 1.38mm, the TR/TE/flip angle varies $4.0 - 4.7/2.0 - 2.6/15^\circ - 60^\circ$, normally using values of $4.1/2.0/45^\circ$.

2.2 Algorithm description

The design of the proposed algorithm is based on the three assumptions listed in the introduction: i) the LV is close of the center of the image, ii) the LV is circular shaped and iii) there is a high temporal variability of the image intensity in the myocardium boundaries due the heart beating.

The algorithm is performed in two steps: in the first step, the center of a fixed-size predefined width ROI is estimated based on the *Hough transform* (HT) (Ballard, 1981); in the second part the center coordinates and width of the previous ROI is refined in and adaptive way.

This ROI is then extended to the entire stack of images over all the cardiac cycle frames, resulting in a 4D cropped image volume.

The algorithm was implemented in Matlab R2007b and in typical conditions spent about 2 minutes for the all processing and loading the final cropped volume.

2.2.1 Fixed-size LV windowing

Let $x(i,j,p,t)$ be the $(i,j)^{th}$ voxel in the p^{th} plane at the t^{th} time frame, where $1 < i,j,k,t < M,N,L,T$. A *standard deviation* (STD) map is computed according to Eq.2.1, using all temporal slices from the middle plane of the short-axis images stack, as displayed in the Results section in Fig.3 (b). As (Cocosco et al., 2004) suggested, high STD is found between the myocardium and the blood-pool. Additionally, this map will introduce extra ringing around the LV borders, i.e., more circular shapes. Therefore, here the *a priori* knowledge of the circular shape is used to locate the LV in the STD map using the HT.

$$STD(i,j) = \sigma_t(i,j) = \sqrt{\frac{1}{T}\sum_t \left(x\left(i,j,\frac{L}{2},t\right) - \mu_t\left(i,j,\frac{L}{2}\right)\right)^2}, \tag{2.1}$$

where $\mu_t\left(i, j, \frac{L}{2}\right)$ is the mean of the signal over the time, estimated in the position $\left(i, j, \frac{L}{2}\right)$. Before calculating the STD map, the images are filtered by a Gaussian mask to reduce the noise. This reduction is important guarantee that the STD map observed is mainly generated by temporal variations and not by spatial noise. The Canny edge detector (Canny, 1986) is then applied to get an edge-map to be used in the circular HT algorithm (see Fig. 3(c)).

The used circular HT algorithm is computed for a fixed radius and the output is an accumulator $\mathbf{Acc}$ with the same dimensions of the input image $[M, N]$. The value at $Acc_r(i, j)$ represents the number of circles with radius r centered at the edge pixels that intersect the $(i, j)^{th}$ pixel. Based on the knowledge that the LV centroid is the center of multiple circles (the ring generated in the STD map and of the epicardial and endocardial border) and that the LV has variable size, the HT is computed for a set of different radius values. The maximum radius of the LV (at the end of the diastole) can range from 18mm to 28mm (Feigenbaum, 2005). Using this interval as reference, the HT was calculated for radius ranging from 15mm to 40mm . The maximum radius was increased to 40mm in order to include the epicardial border of the LV, and the minimum was decreased to 15mm because the middle plane of the stack might not correspond to the largest section of the LV. With steps of 2 mm of interval, the circular HT is processed for all the radius from 15mm to 40mm and the accumulators are added at each step (Eq. 2.2). The $\mathbf{Acc}_{Total}$ incorporates the whole information about circles with every radius in the range, amplifying its common center location. Adding the accumulators will ensure that the maximum will be closer to the centroid of the LV.

$$Acc_{Total}(i, j) = \sum_r Acc_r(i, j) \tag{2.2}$$

Based on the assumption that the LV is always close to the center of the image, the circles detected close to it will be favored. The $\mathbf{Acc}_{Total}$ is then multiplied by a mask that has unitary value in a circular region around the center of the image and with decreasing values up to the borders, following Eq. 2.3 and showed in Fig. 1.

$$h(\mathbf{x}) = \begin{cases} 1 & \text{if } \|\mathbf{x}-\mathbf{c}\| \leq R, \\ \left(\frac{1}{\|\mathbf{x}-\mathbf{c}\|} - \frac{1}{\|\mathbf{c}\|}\right) \cdot R & \text{if } \|\mathbf{x}-\mathbf{c}\| > R, \end{cases} \tag{2.3}$$

where $\mathbf{c} \in R^2$ represents the center of the image, $\mathbf{x} \in R^2$ the position of a mask element and $R = 50$mm, related with human anatomy. This value is fixed and was selected based on experimental tests and on the results from (Pednekar et al., 2006). This reference radius determines the maximum possible distance from which the LV centroid is apart from the center of the image and the circular region where the $\mathbf{Acc}_{Total}$ has unitary weight. Outside this region the $\mathbf{Acc}_{Total}$ is weighted by smaller values, reducing the importance of the detected circles in this area. The mask is zero at the corners of the image.

The new ROI is squared and centered at the coordinates of the maximum of the $\mathbf{Acc}_{Total}$. The side dimensions of this bounding box were set to $(2+\epsilon)r_{max} = 120$ mm, where $\epsilon = 1$ is a safety coefficient and $r_{max} = 40$ mm.

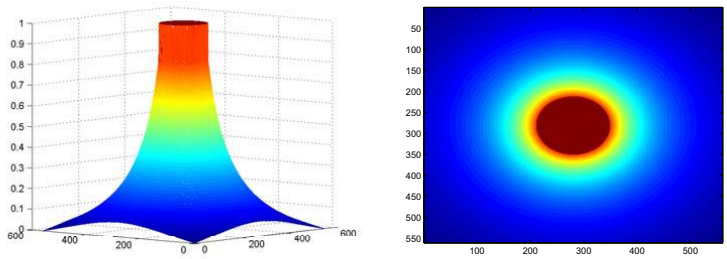

(a) (b)

Figure 1: Accumulator mask that used to reducing the importance of the detected circles outside the centered circular region. (a) 3D view (b) top view.

2.2.2 Adaptive LV windowing

In the first step of the algorithm a fixed size bounding box is generated, only depending on the pixel resolution. In the second step, the window size and center will be adapted using the previously estimated bounding box as a starting point.

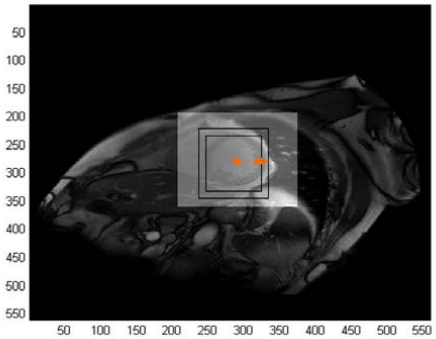

Figure 2: Growing bounding box. The orange arrows represent the direction of the increase of the side of the window.

A growing bounding box centered on the previously estimated window is used (see Fig. 2). The box size increases from $2r_{min} = 30$ mm to $3r_{max} = 120$ mm, with 10 mm gap between iterations. Let $D(k)$ be the width of the box at k^{th} step of the growing bounding box and $\mathbf{x} \in R^2$ a position in the accumulator matrix. The new parameters to generate an adaptive window are estimated by Eq. 2.4. The range of radius used in the first step is also used here. The new squared bounding box is centered at $\mathbf{c}_{adaptive}$ and with width $(2+\epsilon)r_{adaptive}$, where $\epsilon = 1$ is a safety coefficient.

$$(r, \mathbf{c})^{new}_{adaptive} = \arg\max_{r,\mathbf{x}} \mathbf{Acc}_{r,D(k)}(\mathbf{x}) \tag{2.4}$$

In Fig. 7 it is possible to observe an example of the relation between the radius and the maximum of $\mathbf{Acc}_D$ for a given D size of the growing bounding box.

3 Results

The algorithm was tunned and tested by using the images acquired from 17 patients. The R value was set to 50mm and the parameters used in Canny edge-detector are automatically selected by the algorithm. The improvements in reduction of the image size are presented in Tab. 1. The contents of the estimated bounding box for all the data-sets were visually inspected for every slice over all time frames for both steps of the algorithm.

Table 1: Size of the cropped region compared to the original image at the end of each step of the algorithm.

Patient	Fixed-Size	Adaptive $\epsilon = 1$
A	30.0%	23.0%
B	30.5%	23.4%
C	30.0%	23.0%
D	32.4%	25.6%
E	28.1%	25.3%
F	30.0%	28.4%
G	30.0%	27.9%
H	30.0%	29.5%
I	30.0%	29.5%
J	25.4%	23.7%
K	26.3%	21.5%
L	30.0%	29.5%
M	30.0%	28.9%
N	30.0%	23.0%
O	30.2%	29.7%
P	30.0%	27.3%
Q	34.0%	32.8%

All the tested data-set had successful results, *i.e.*, the LV was always within its borders (see Fig.3 as example). Although most of the data-sets presented some misalignment between consecutive planes (see. Fig. 4), the LV endocardial and epicardial borders were always inside the estimated fixed-size window.

The size of the cropped images is equal to 30.0% of the original image in most of the cases, 25.4% in the best case and 34.0% in the worst case (see Tab.1). In this step, the reduction only depends on the resolution of the image.

In Fig.3 it is possible to see an example of the results from patient Q. In the STD map it is clear the ringing effect resulting from alternating high and low STD areas due to muscle contraction and in the Canny edge-map it is possible to see circular structures in the LV region. In the

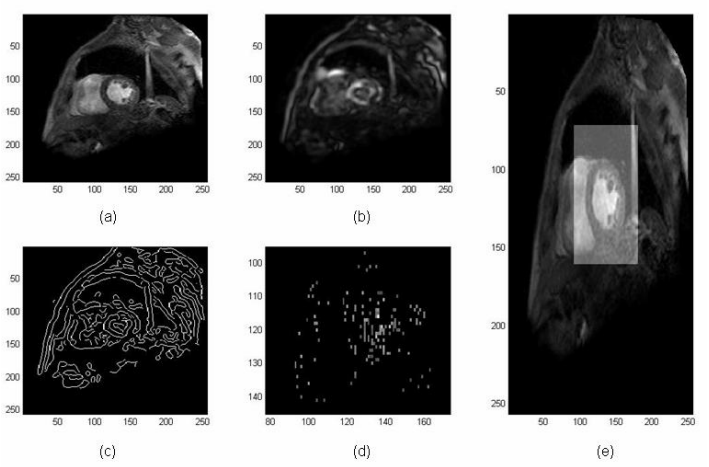

Figure 3: Results from patient Q. (a) original image (middle slice 2nd time-frame); (b) STD map; (c) Canny edge-map; (d) Filtered accumulator map, zoomed into the area where the accumulator has higher intensity; (e) Resulting bounding box highlighted in the original image.

accumulator map it is possible to identify the brighter pixel close to the LV center (around 140 in the x direction and 120 in the y direction). In the last image it is possible to observe the fixed-size window generated in the first step of the algorithm.

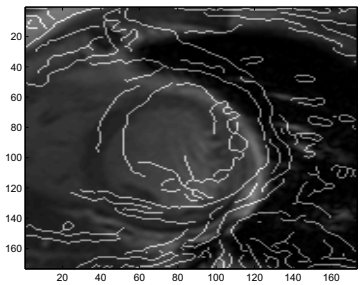

Figure 4: Misalignment between consecutive slices in the same time frame for patient A - Overlay between original bounded 4^{th} plane and bounded Canny edge-map from original 5^{th} plane

There were only two patients where the algorithm did not performed as expected. Despite the whole LV is inside the bounding box, the LV centroid is slightly away from its center (see Fig. 3).

Significantly improvements were also observed with the adaptive LV windowing, where in most the data-sets ($13/17$) the initial bounding box was reduced and centered closer to the centroid

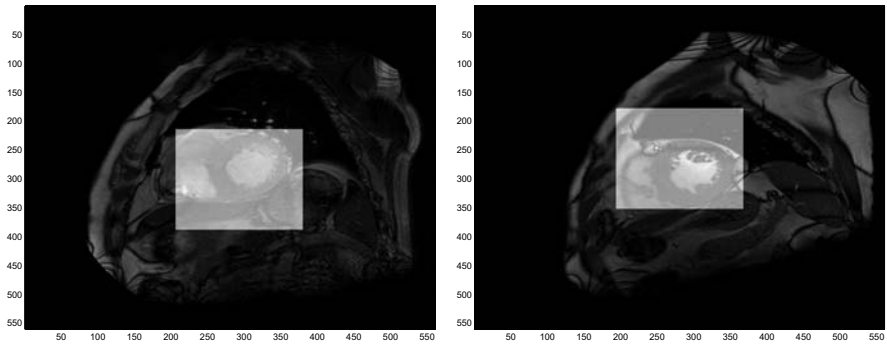

Figure 5: Not centered results. (a) Patient H (b) Patient I.

of the LV (see Fig.6). The window size was first set to $3r_{adaptive}$ where ϵ was set to 1.

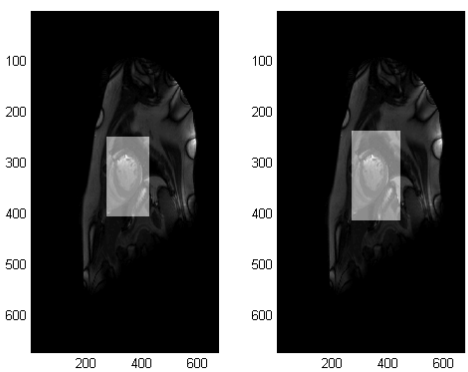

Figure 6: Windowing results from patient J (a) Adaptive LV windowing; (b) Non-adaptive LV windowing.

In the 4 unsuccessful data-sets (some examples shown in Fig. 7) the bounding box was not enough to enclose the entire LV borders. An increase of the constant factor to 3.5 eliminates this effect, but the resulting bounding box is normally slightly larger (1% to 2%) than the one from the first step of the algorithm.

In Fig. 7 it can be observed that the unsuccessful results, such as Fig. 7 (b) correspond to a sharper peak in a smaller radius in Fig. 7 (b), while the successful ones correspond to a peak for higher radius, as in Fig. 7 (a).

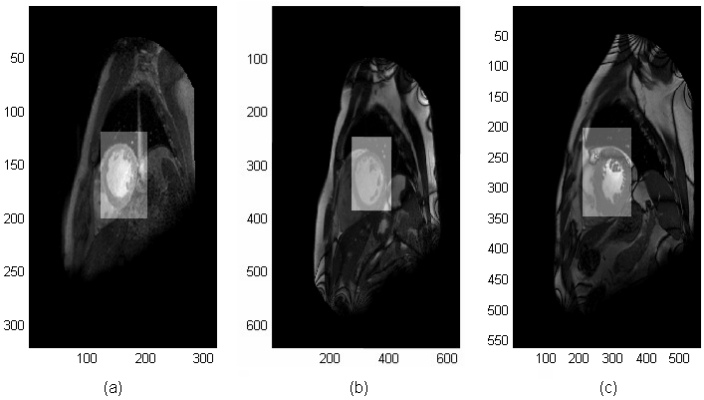

Figure 7: Thigh results from adaptive LV windowing (a) Patient E; (b) Patient K (c) Patient I.

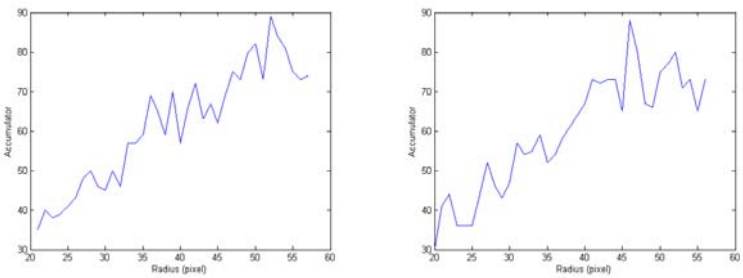

Figure 8: Graphics from biggest bounding box, radius vs accumulator. (a) Patient J (b) Patient K.

4 Discussion

LV function is assessed by using short-axis cardiac cine-MRI that represent large amounts of data: 10 up to 17 volume images over 15 up to 30 frames in the cardiac cycle. This data is inspected manually by the expert and contours are drew manually to extract the EF value. It is a time consuming process and its full automatization is of great interest.

One of the most successful method described in (Cocosco et al., 2004) is based in the high temporal variability of the image intensity in the myocardium boundaries where they are able to compute a *region of interest* (ROI) by using 79 cine cardiac structural MRI clinical scans without leaving out any part of the myocardium. The main drawback of this algorithm is to have two tunable parameters on which it depends. However, the authors were able to find some proportionality with the voxel size which makes this tunning automatic for typical adult heart dimensions.

Other approach proposed in (Müller et al., 2005) uses a size invariant circular HT (Ballard, 1981) to calculate the ROI and locate a point in the LV endocardium in a previously segmented

image. The method performed successfully for all the 31 MRI recordings. They use Otsu's method followed by a morphological operator to segment a connected region where the point calculated by the HT will fall. This method does not take into account the signal change along the slice which makes the thresholding method less robust.

The short-axis images typically have 512×512 pixels covering a FOV containing the heart and much more. Reduction of matrix dimension is an important first step to exclude unrelevant information and speed up the processing tasks.

This paper presented a fully automated crop function that successfully performed this task over the data from 17 patients.

As previously mentioned, the signal intensity is not constant over the volume due to differences in the sensitivity along the coil and also along the slice due to cardiac flow dynamics (Pednekar et al., 2006). This algorithm proved to be robust to signal variation over the image, which is usually a difficulty that must be dealt with. The proposed algorithm is able to cope with this problem because it does not depend directly on the original image but on the STD map, which decreases its sensitivity to these fluctuations and provides edge maps that contain all ringing information required for the success of the circular HT, which is robust to fragmented contours.

Furthermore, cine-MRI are acquired along several breath-holds from the patient, in order to prevent respiratory motion artifacts. This can lead the misalignment of the LV along the stack (Holland et al., 1998) if the subject is not able to hold its breath properly during each volume acquisition time slot. Although the algorithm only takes the middle slice to calculate the bounding box, it has proven to be robust to plane misalignment, mainly because they are usually small and the cropped window is big enough to fit them.

It is not, however, able to consistently locate the exact center of the LV because usually it is not a trivial task to define it. This is shown in the results from patient H and I in Fig. 3. Although the center was not located successfully, the center of the bounding box is close enough from the LV centroid. This algorithm located another circular structure close to the LV, like the myocardium that encloses the LV and the right ventricle, who's center is close to the LV.

The results obtained in the first step of the algorithm can be improved in the second step, where a window-size refinement is performed.

With a $\epsilon = 1$ it was possible to see that in a few cases the LV was not completely enclosed by the bounding box. However, in these cases a clear peak could be observed in the graphics as the ones presented in Fig. 7 (b), in opposition to most of the successful cases where the peak was located at higher radius. This peak represents a clear increase of the accumulator, identifying circular shape for a given radius, in contrast to the biased increase in the accumulator value with the increase of the radius. A proper filtering of this graphic could improve the radius selection and, therefore, a refined bounding box.

Further reduction might be possible once the images are aligned and the centroid of the LV is properly identified.

5 Conclusions

LV contour extraction and tracking is important in diagnosis of cardiac pathologies. In the clinical routine, this procedure is performed manually using software assistance, a time consuming process and presents high intra/inter operator variability. Its automatization is of great importance to the clinical practice.

The large amount of data of these cine-MRI exams requests a dimension reduction into a ROI that encloses entirely the LV over the stack and over all the time frames acquired in order to reduce the computational burden associated with the pre-processing and segmentation algorithm.

In this paper it was proposed an algorithm to automatically crop based on the well known Hough transform for circles, in the prior knowledge about the location of the heart and also on the high signal variability over time due to muscle contraction at the LV borders.

This algorithm was tested over 17 data-sets of cine-MRI from patients with cardiac pathologies where the LV function was accessed. The first step of the algorithm provided a reduction to a squared ROI with width equal to 30% of the original images. Promissing results were also achieved in the second step of the algorith, where it was possible to increase the reduction but still with a few limitations.

The performance of this algorithm was compared with state of the art algorithms ((Müller et al., 2005) and (Cocosco et al., 2004)) but there where no quantitative data available about the reduction accomplished. However, this crop algorithm seems to be more robust to the difficulties presented by these exams.

Reduction of dimension if of great importance for the tasks that follow in the segmentation of the LV: alignment and segmentation. Here is presented an automated crop procedure, which opens the door to a fully automated segmentation of the LV.

Acknowledgment

All the clinical data used for this work was supplied by Sociedade Portuguesa de Ressonância Magnética. The circular HT algorithm was implemented by (Amin, 2004).

References

Amin, S. 2004. Circular hough transform algorithm, *Photogrammetry and Computer Vision Devision, Geomatics Department,Faculty of Engineering, University of Tehran,Iran* .

Ballard, D. H. 1981. Generalizing the hough transform to detect arbitrary shapes, *Pattern Recognition* **13**(2): 111–122.

Canny, J. 1986. A computational approach to edge detection, *Pattern Analysis and Machine Intelligence, IEEE Transactions on* **PAMI-8**(6).

Cocosco, C. A., Netsch, T., Sénégas, J., Bystrov, D., Niessen, W. J. and Viergever, M. A. 2004. Automatic cardiac region-of-interest computation in cine 3d structural mri, *CARS* pp. 1126–1131.

Feigenbaum, H. 2005. *Feigenbaum's echocardiography*, PA: Lippincott, Philadelphia.

Holland, A., Goldfarb, J. and Edelman, R. 1998. Diaphragmatic and cardiac motion during suspended breathing: preliminary experience and implications for breath–hold mr imaging, *Radiology* **209**: 483–489.

Katouzian, A., Prakash, A. and Konofagou, E. 2006. A new automated technique for left- and right-ventricular segmentation in magnetic resonance imaging, *Engineering in Medicine and Biology Society, 2006. EMBS '06. 28th Annual International Conference of the IEEE* pp. 3074–3077.

Müller, A., Neitmann, A., Merkle, N., Wohrle, J., Hombach, V. and Kestler, H. 2005. Contour detection of short axis slice mr images for contraction irregularity assessment, *Computers in Cardiology* pp. 21–24.

Nascimento, J. C. and Marques, J. S. 2008. Robust Shape Tracking with Multiple Models in Ultrasound Images, *IEEE Transactions on Image Processing* **17**(3): 392–406.

Nascimento, J. and Sanches, J. 2008. Ultrasound imaging lv tracking with adaptive window size and automatic hyper-parameter estimation, *Proceedings IEEE ICIP 2008*, 2008 IEEE International Conference on Image Processing, San Diego, California, U.S.A.

Pednekar, A., Muthupillai, R., Lenge, V., Kakadiaris, I. and Flamm, S. 2006. Automatic identification of the left ventricle in cardiac cine-mr images: Dual-contrast cluster analysis and scout-geometry approaches, *Journal of Magnetic Resonance Imaging* **23**: 641–651.

Wu, K. and Lima, J. 2003. Noninvasive imaging of myocardial viability: current techniques and future developments, *Circulation Research* **93**: 1146–1158.